Commun. Fac. Sci. Univ. Ank. Series A2-A3
V. 44. pp. 1-16 (1997)

MIXING PROPERTIES OF A VISCOELASTIC FLUID
Part I: In A 2D Cavity Flow

Hüseyin DEMİR

Department of Mathematics, Ondokuz Mayıs University, Faculty of Education, Atakum/Samsun, TURKEY.

(Received Oct. 6, 1997; Accepted Dec. 31, 1997)

ABSTRACT

The laminar flow of Newtonian and non-Newtonian fluids with constant and variable shear-rate parameters are studied theoretically. Numerical solutions for the concentration, velocity, particle path are obtained using finite differences and A.D.I. method in 2D cavity. Mixing properties are investgated by tracking the motion of a number of selected fluid particles and by simulating the dispersive mixing of a 'coloured' fluid injected into the cavity while at rest. The stability of concentration intensity is investigated for a wide range of Newtonian and non-Newtonian fluids. The effects of inertia and elasticity are of particular interest. The instabilities are characterised by control parameters: the Reynolds, Weissenberg and Schmidt numbers.

1. INTRODUCTION

This paper is aimed to make a contribution to the study of the mixing of viscoelastic fluids at Re=1 and Re=100. Such mixing of viscoelastic fluids is a commonly used but is not well understood in the industrial processing of the fluids due to difficulties that occur with computing the velocity field [1] and these difficulties make the analysis of mixing flow very complicated. Both Newtonian and non-Newtonian fluids are considered for the concentration results and the dispersive mixing generated by the flow patterns of the cavity flows. Furthermore it is assumed that the dye initially occupies the half of the cavity and there is no chemical reaction in the concentration flow equation. Results for fluid particle speed and concentration results are obtained by numerical simulation.

2. THEORY

The governing equations of motion are applied to driven cavity flow. Cartesian (x,y) co-ordinate system are taken with velocity vector $V_i = (u,v)$, the driven cavity geometry is shown in Figure 1 with gravity acting vertically.

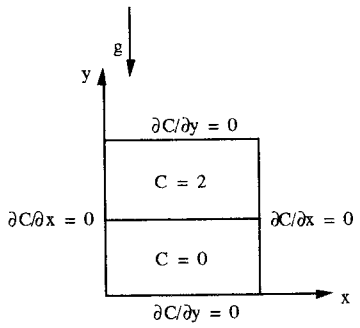

Figure 1. Flow Geometry, Boundary Conditions and initial condition for Concentration Dispersion

Non-dimensionalising by writing

$$x' = x/\ell,\ y' = y/\ell,\ u' = u/U,\ v' = v/U,\ \omega' = \ell\omega/U,\ t' = tU/\ell,$$

$$\psi' = \psi/U\ell,\ \dot{\gamma}' = \dot{\gamma}/U \quad \eta' = \eta/\eta(0),$$

where the dashed notation "$(\bullet)'$" is the non-dimensionalised variable, U is a characteristic velocity, ℓ is a characteristic length, u and v are the velocity components in x and y direction respectively, η is the viscosity, ω the vorticity, ψ the stream function, t is the time and $\dot{\gamma}$ the shear-rate. For convenience from now on we shall omit the dashes after the non-dimensionalisation process.

Subsequently, for the relation between the stres tenser σ_{ik} and the velocity we choose the Criminale-Erickson-Filbey (CEF) [2] fluid model with equation of state

$$\sigma_{ik} = 2\eta(\dot{\gamma})\ d_{ik} + 4\chi(\dot{\gamma})d_{ij}d_{jk} - 2\xi(\dot{\gamma})\overset{\nabla}{d}_{ik}\ , \tag{1}$$

where $\eta(\dot{\gamma})$ is the solvent viscosity, $S_{ik} = 4\chi(\dot{\gamma})d_{ij}d_{jk} - 2\xi(\dot{\gamma})\overset{\nabla}{d}_{ik}$ is the polymeric part and modelled by the Criminale-Erickson-Filbey (CEF) (7), d_{ik} is defined as rate of strain tenser. Now $4\chi(\dot{\gamma}) = \frac{1}{2}N_1(\dot{\gamma}) + N_2(\dot{\gamma})$, $2\xi(\dot{\gamma}) = N_1(\dot{\gamma})$, where $N_1(\dot{\gamma})$ and $N_2(\dot{\gamma})$ are known as the primary and secondary normal stress coefficients, respectively. Since we work with the CEF model $\dot{\gamma}, N_1, N_2$ completely determine the state of stress in a rheological shear flow. It remains only to define the upper convected derivative in equation (1) as;

$$\overset{\nabla}{d}_{ik} = \frac{D}{Dt}d_{ik} - Ld_{ik} - d_{ik}L^T \tag{2}$$

where

$$\frac{D}{Dt}(\bullet) = \frac{\partial}{\partial t}(\bullet) + (V_i.\nabla)(\bullet) \text{ and } L = \nabla V_i \text{ and } L^T = (\nabla V_i)^T .$$

Depending on the form of the variable viscosity $\eta(\dot{\gamma})$ equation (1) yields the viscosity function model such as the Cross model which is given by:

$$\eta(\dot{\gamma}) = \eta(\infty) + \frac{(\eta(0) - \eta(\infty))}{1 + (\lambda\dot{\gamma})^{1-n}} \tag{3}$$

In this model $\eta(\infty)$ represents the infinite shear viscosity for very large deformation rates, and $\eta(0)$ represents the zero shear rate viscosity for very small rates of shear.

The equations of motion of unsteady incompressible flow of a CEF fluid with shear-rate dependent viscosity may be written as:

$$\frac{\partial\omega}{\partial t} = \frac{1}{\eta Re}H(\eta^2;\omega) - \eta\left\{u\frac{\partial\omega}{\partial x} + v\frac{\partial\omega}{\partial y}\right\} + \frac{1}{Re}F \tag{4}$$

$$\omega = \nabla^2\psi, \tag{5}$$

where

$$H(\eta^2;\omega) = \left\{\frac{\partial}{\partial x}\left(\eta^2\frac{\partial\omega}{\partial x}\right) + \frac{\partial}{\partial y}\left(\eta^2\frac{\partial\omega}{\partial y}\right)\right\} \tag{6}$$

$$F = M(\psi)M(\eta) + L(\psi)L(\eta) - \frac{1}{2}M\{S_{xx} - S_{yy}\} - L\{S_{xy}\} \tag{7}$$

Here Re represents Reynolds' number which is defined as $Re = \rho U\ell/\eta(0)$.

The concentration equation becomes

$$\frac{DC}{Dt} = \frac{1}{ScRe}\nabla^2 C \tag{8}$$

where Sc represents the Schmidt number and describes the relationship between the viscosity and the molecular diffusity (K_c), with Sc defined as:

$$Sc = \eta(0)/\rho K_c. \tag{9}$$

Eqations (4)-(5) and (8) will be solved by the stream function and vorticity approach. The boundary conditions are shown in Figure 1. For the concentration equation we employ the homogenos Neumann type boundary for impermeable walls. We use the gradient or flux condition at every point of boundary which is $\frac{\partial C}{\partial n} = 0$, where n is outward normal. The dye is "injected" into the top half of the cavity within which the fluid is initially at rest. Subsequently we 'observe' how the concentration intensity varies with respect to time, due to fluid motion. We choose the overall concentration in the area (A) to be unity. Therefore, we have

$$\iint_A C(x,yt)dA = 1 \tag{10}$$

The integral is evaluated numerically to second order by using the trapezium rule.

The other consideration for the concentration equation is the initial condition. The ordinary differential equations of particle paths are given in the following system with respect to Cartesian co-ordinates (x,y)

$$\frac{d}{dt}\underline{x}_i(t) = V_i(\underline{x}_i(t)) \tag{11}$$

where i = 1,2, x_1 = x and x_2 = y. The variable V_i represents the velocity components in the x and y direction, respectively. The above system is considered with initial conditions $x(0) = x_0$ and $y(0) = y_0$. The velocity field is obtained numerically by the initially setting starting points (x_i,y_i) and then proceeding with the solution through using $u = -\frac{\partial \psi}{\partial y}$ and $v = \frac{\partial \psi}{\partial x}$. The solution is obtained to $O(\Delta t^2, h^2, k^2)$ in the A.D.I. method. or this approaches we employ the second order modified-Euler method [3] to track particles. We formulate the Euler method by re-arranging (11) initial conditions to obtain

$$\underline{x}_{i+1} = \underline{x}_i + \frac{\Delta t}{2}\left[V^0(\underline{x}_i) + V^N(\underline{y}_i)\right] \tag{12}$$

where $\underline{y}_i = \underline{x}_i + \Delta t V^0(\underline{x}_i)$. The system uses known values of V^0 and V^N which are old and new values of the velocity components respectively.

3. THE FINITE DIFFERENCE METHOD

Taking a grid defined by

$$x_i = i\Delta x \qquad i = 0, 1, ..., M \tag{13}$$

$$y_j = j\Delta y \qquad j = 0, 1, ..., N \tag{14}$$

where Δx and Δy denote the grid spacing in the x and y directions, respectively and also $t = n\Delta t$, $n = 0, 1$ ... with Δt as the time increment where n is the number increments needed to reach some desired time $n\Delta t$. For simplicity, we call $\Delta x = h$ and $\Delta y = k$ and so $h = \frac{X_M}{M}$, $h = \frac{Y_N}{N}$, where X_M and Y_N represent the height and width, respectively. The quantity $\alpha = \frac{k}{h}$ is defined as the grid aspect ratio of the cavity.

We have the equatinos (5, 6, 8) which will be discretised by using finite differences approximation. The stream function-vorticity equation can be expresed in a standart notation as

$$B_1\psi_{i,j} = B_2\psi_{i+1,j} + B_3\psi_{i-1,j} + B_4\psi_{i,j+1} + B_5\psi_{i,j-1} + B_6 \tag{15}$$

where the coefficients in equation (13) become

$$B_1 = 2(\alpha + 1),\ B_2 = B_3 = \alpha^2,\ B_4 = B_5 = 1 \text{ and } B_6 = k^2\omega_{ij}\ .$$

On using the A.D.I. [4, 5] method to solve the time-dependent equations by using standart central differences with $r = \frac{\Delta t}{h^2}$ and $s = \frac{\Delta t}{k^2}$ as

$$\left(1 - \frac{r}{2}L_x^h\right)\Phi^* = \left(1 + \frac{s}{2}L_y^k\right)\Phi^n + \frac{\Delta t}{2}f_n\ , \tag{16}$$

$$\left(1 - \frac{s}{2}L_y^k\right)\Phi^{n+1} = \left(1 + \frac{r}{2}L_x^h\right)\Phi^* + \frac{\Delta t}{2}f_n\ . \tag{17}$$

Here L contains space derivatives and $L = L_x + L_y$, with L_x having only x derivatives and L_y only y derivatives. Let Φ^n be the value of ω at $t = n\Delta t$ and Φ^{n+1} that at $t = (n + 1)\Delta t$. Also Φ^* denotes intermediate approximation between old time t and the new time $t + \Delta t$. For a PDE, such as the vorticity and concentration equations, the error due to

discretsion is found to be second order in both time and space. The finite difference method gives to rise to systems of non-algebraic equations. We let **Ax = b** denote the non-linear algebraic equations, with **A**, an **NxN** matrix, **b**, **Nx1** column vector of given, and **x**, **Nx1** vector of unknowns interior mesh values. However, the method yields a pair of implicit equations. The solution of each equation is obtained through the Gaussian Elimination direct type method which is well explained in Smith [6].

4. RESULTS

All results are produced for the time-dependent viscous and visco-elastic fluid flow for the dispersive mixing generated by the cavity flow. In the 2D numerical simulation, we first considered the convergence properties of the numerical solutions by comparing calculations for various grid widths denoted by h. On comparing values of concentration we had evidence that convergence to 4 decimal places has been achieved for Re=1 and Re=100 and where Schmidt number is taken as 50. Figure 2 shows result for the convergence of the concentration test criterion with respect to the mesh size. As seen, while the mesh size decreases the convergence values decrease as well. In this case the results are acceptable as long as the time increment is sufficiently small.

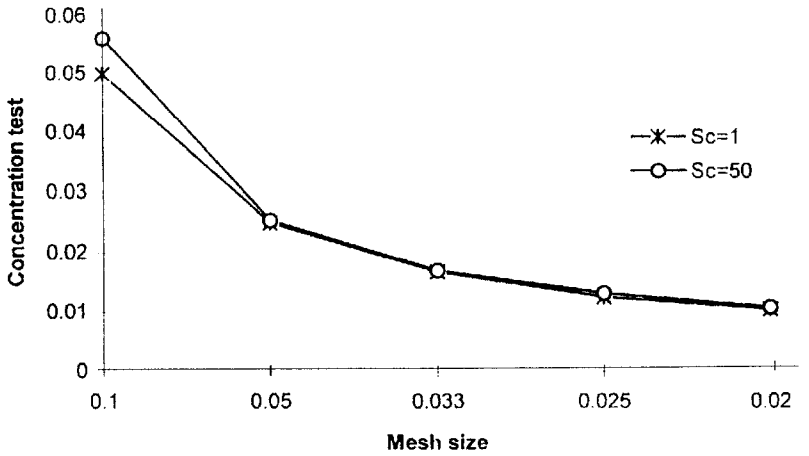

Figure 2. Convergence Criterion for concentration test problem

A second comparison is a graphical comparison of centre line **u**-velocity, which is the x component of velocity vector, for a Reynolds number of 100 and 1000 for both Newtonian and non-Newtonian fluids. In the literature only Newtonian fluid data was found with which to compare our results. Our results agree very well with Tosoka et al. [7] both qualitatively and quantitatively as seen in figure 4. In addition, non-Newtonian pseudoplastic result were obtained at Re=100 and Re=1000 and displayed and interesting and significant change from the Newtonian case.

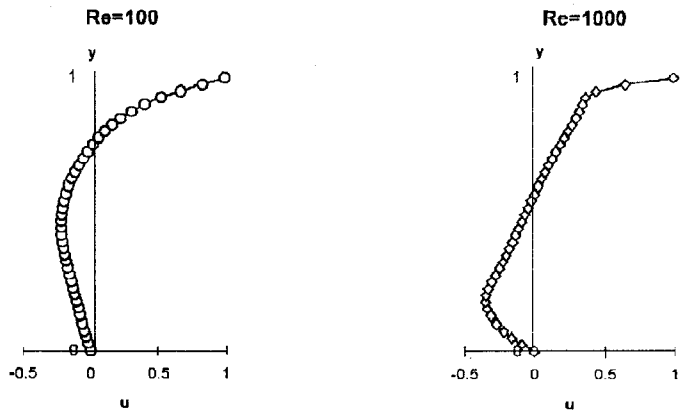

Figure 3a. u velocity profile along vertical centre line at Re=100 and Re=1000 for Newtonian fluid.

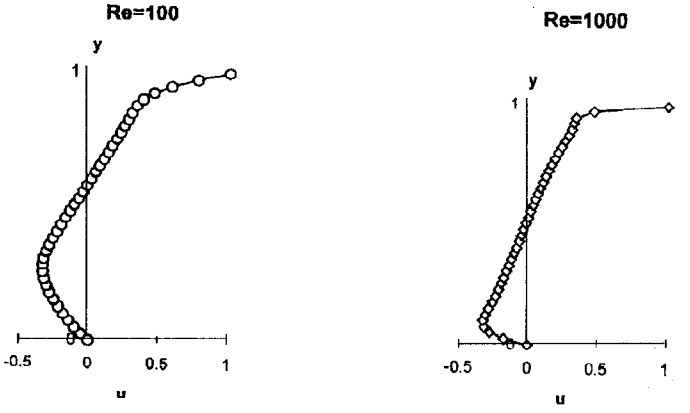

Figure 3b. u velocity profile along vertical centre line at Re=100 and Re=1000 for pseudoplastic fluid.

Before summarising the results for each case, we shall explain how the flow of shear-thinning and shear-thickening, viscous an visco-elastic fluids were simulated. For the shear-thinning fluid the zero shear viscosity is taken as 1 and the infinite viscosity is taken 0.1, and vice versa in the case of shear-thickening fluids. We organise all results for concentration field in terms of the following cases.

1) Standart cavity driven flow with the top wall moving
2) Two walls moving in the opposite direction
3) Two walls moving in the same direction.

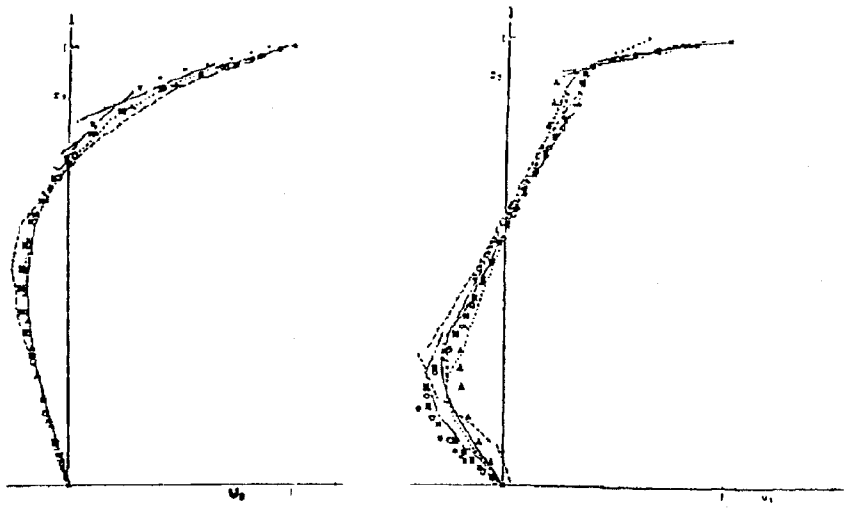

Figure 4. Comparison of u velocity profiles along vertical centre line at Re=100 and Re=1000. Tosaka et al..

4.1. Standart Cavity Driven Flow

In this case, when Re=1 both viscous and viscoelastic fluids exhibit similar behaviour. A figure is presented for Newtonian fluid below. When non-Newtonian and Newtonian cases are compared it was seen that the non-Newtonian fluid streamlines are located in a relatively higher position in the flow domain. This is because the shear-thinning fluid moves more

rapidly near the top plate where the fluid is tinner. In contrast for the dilatant fluid streamlines are lower than the Newtonian case and the fluid is slower moving near the top plate.

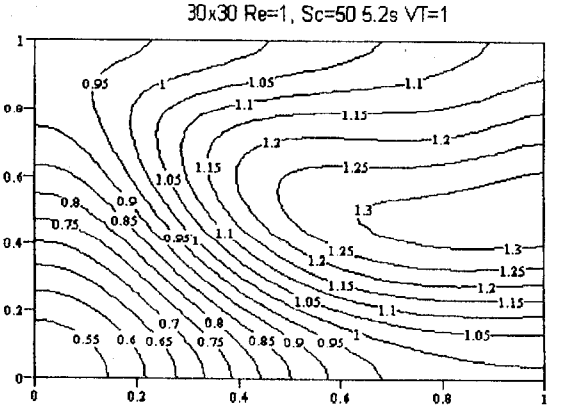

Figure 5. Concentration contours for Newtonian flow at Re=1, Sc=50.

For Re=100 the advection force is more dominant in the concentration equation. In this case the seperation of the coloured band becomes an interface like, and concentration is therefore high near the top plate. The results for non-Newtonian fluids are similar to the Newtonian fluid, except the coloured band is a little higher in the cavity ad less spread out near the top plate. We present a figure for Newtonian at Re=100 below.

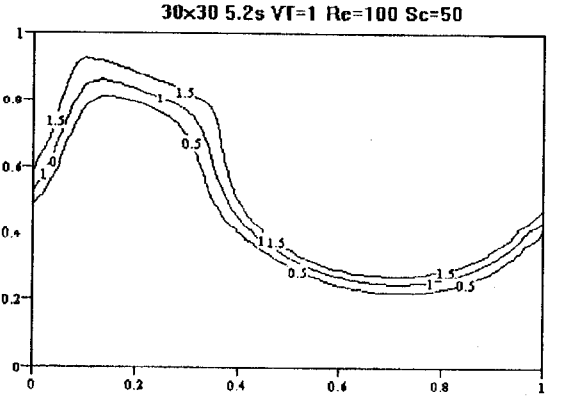

Figure 6. Concentration contours for Newtonian flow at Re=100, Sc=50.

4.2. Two Walls Moving in Opposite Direction

In this case both viscous and viscoelastic fluids are examined with constant and variable shear-rate. All fluids showed little difference when compared to Newtonian case shown in figure 7. The contours indicate that the concentration intensity are more wave like in appearance, and they are almost seen to be symmetric about the positive diagonal (y = x) of the cavity. For Re=100 the advection terms again dominate in the concentration equation. Moreover in the pseudoplastic case the location of the coloured band is higher in the cavity and less spread out near the top wall.

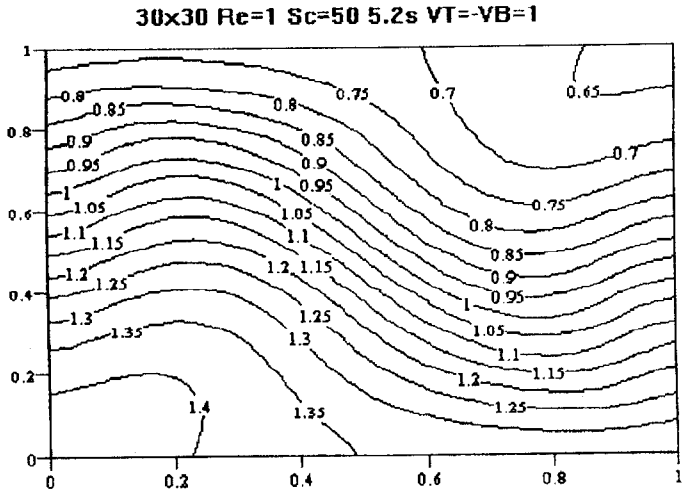

Figure 7. Concentration contours for Newtonan fluid at Re=1, Sc=50.

4.3. Two Walls Moving in the Same Direction

For Re=1 the concentration contours are shown below; they are almost symmetric about the horizontal mid-line of the flow domain in appearance and yet the concentration values are roughly twice as high in the top half of the cavity than in the lower half.

For Re=100 the advection forces dominate the flow and the concentration intensity spread out in the 'slow' flow region and this is

easy to see from figure 9. Here the concentration is slightly more spread out near the left wall because the circulation is weaker and diffusion effects are greater as compared to the right wall. All fluids considered for both viscous and viscoelastic cases produced very similar results, comparatable with a viscoelastic dilatant fluid shown in figure 9.

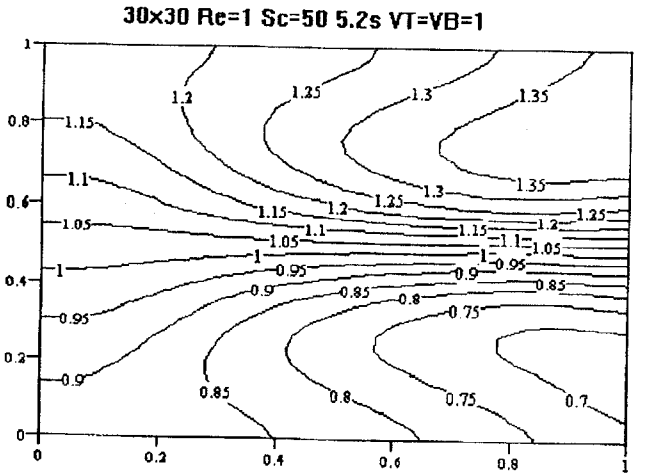

Figure 8. Concentration contours for Newtonian fluid at Re=1, Sc=50.

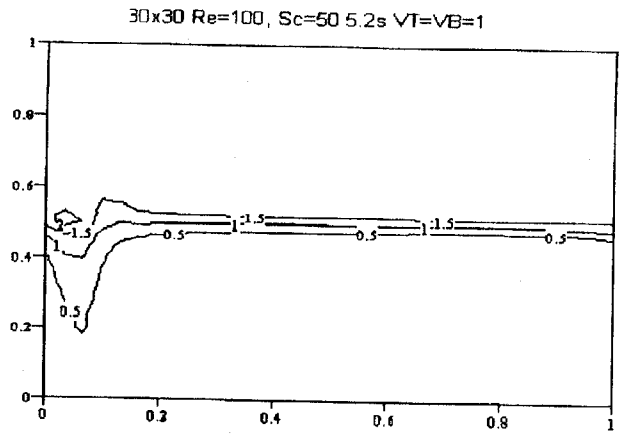

Figure 9. Concentration contours for viscoelastic dilatant fluid at Re=100, Sc=50.

4.4. Particle Paths And Discontinuous Periodic Cavity Flow

In this section particle paths are investigated by using a discontinuous periodic motion with two wall motion as the top and bottom plates move with a periodic motion as shown in figure 10. This motion was firstly investigated by Aref [8] within a cylindirical configuration for incompressible fluid. This solution depends on the period of the motion (T), and on the Reynolds number Re. At first the top wall moves to the right for a period of T. Then its stops and the bottom wall starts moving in the opposite direction for a duration of T. This cycle is repeated until the desired number of times. The flow is simulated for a duration of 60 seconds for two different periods T=1 and T=2. Furthermore, there were three particles considered initially located in the cavity's vertical middle line (x = 0.5).

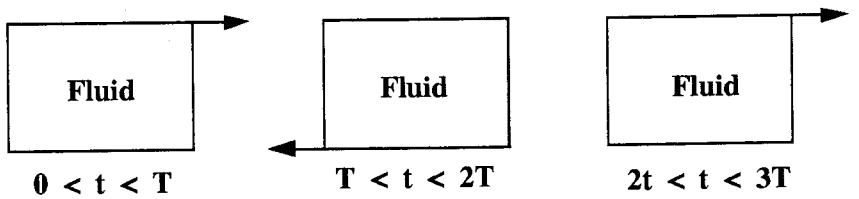

Figure 10. Discontinuous periodic motion for cavity flow

For a Newtonian fluid at Re=1 the trace paths of three particles are shown in figure 11. The outer particle (top figure) paths travel a wider orbit in the cavity. However, all three particle paths become flatter near the cavity's top wall. The middle and lower figures show the traces obtained for the periodic motion of the particles by considering the x and y positions with time. Similar behaviour is obtained for the non-Newtonian fluids as compared with Newtonian fluid. Later we produced results at Re=100 and it was seen that the fluid particle paths tend to become flatter near the top wall due to the increase in the fluid inertia. Also all three particles were seen that move quickly and travel wider distances in the cavity. Moreover, the outer particle path become more 'tightly bound' as shown in figure 12 for a viscoelastic fluid.

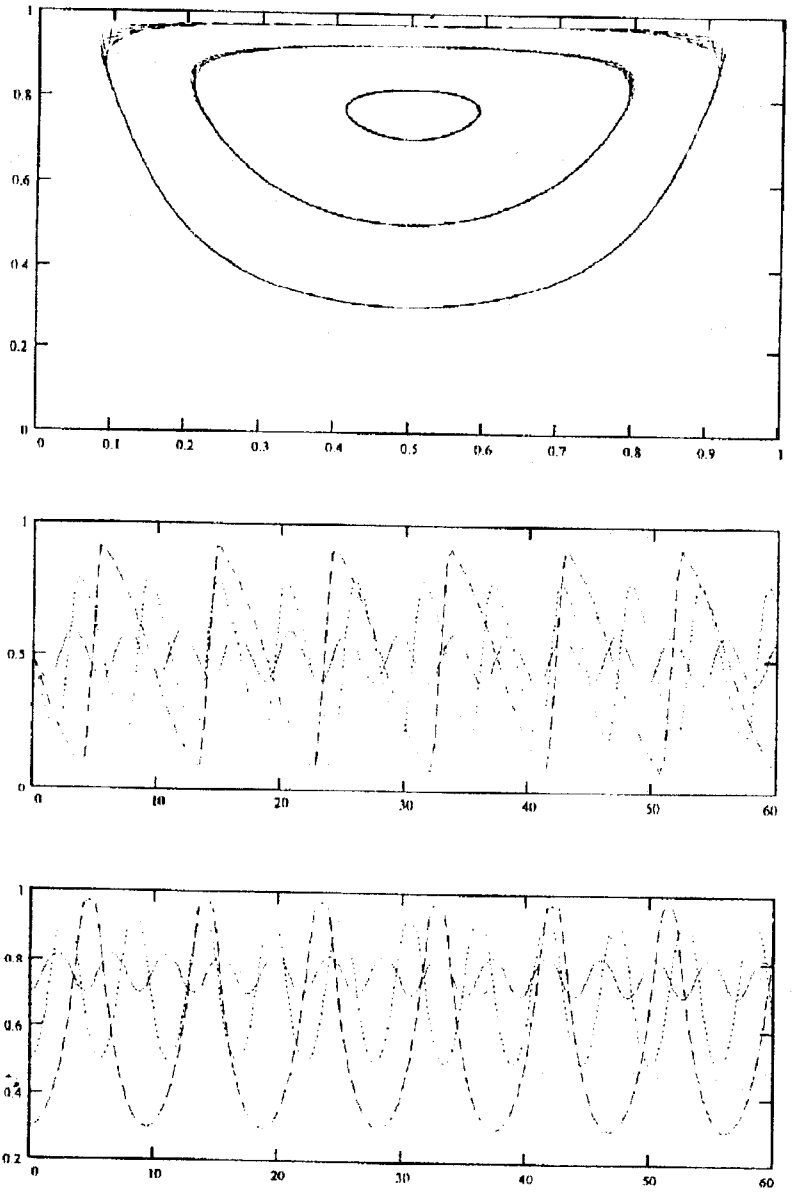

Figure 11. Re=1, Newtonian fluid after 60s, T=1s Initially placed in vertical line.

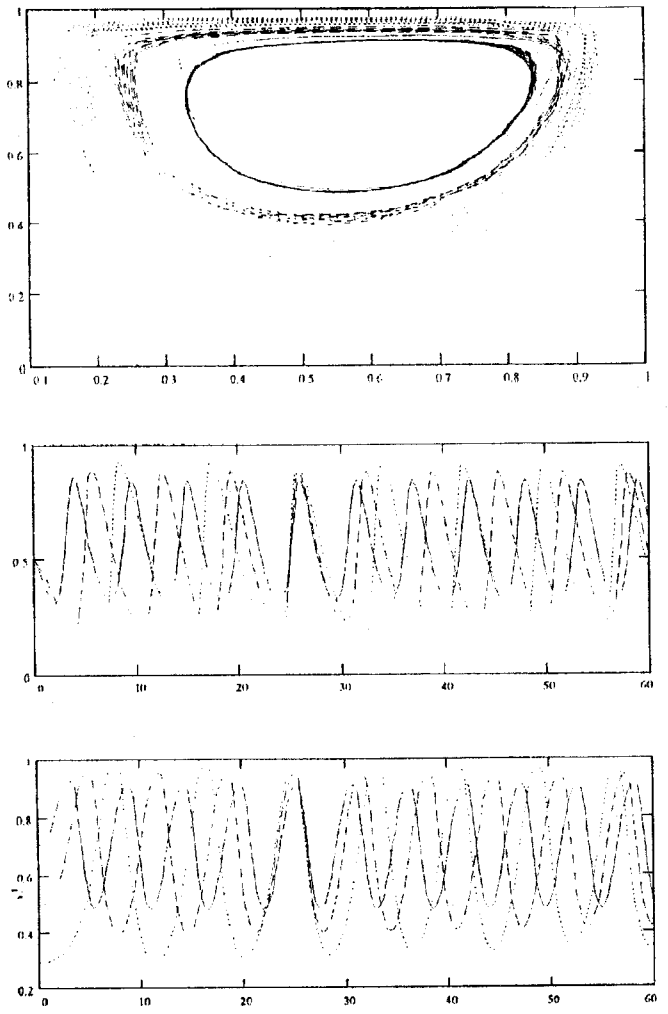

Figure 12. Re=100, viscoelastic dilatant fluid after 60s, T=2s Initially placed in vertical line

5. CONCLUSION

The computational analysis indicates that the scrutimisation of mixing behavior of viscoelastic fluids using a cavity flow domain on a discretised fields is possible within an acceptable amount of error associated with the numerical technique used. In this study, the flow was investigated from

two view points: firstly by analysing the dispersive mixing of a 'coloured' portion of the fluid 'injected' into cavity at rest and secondly by the tracing of a number of selected fluid particles within the flow field. The flow process is very stable for low Re and as Re number increases the advection term starts dominating the flow. It is therefore shown that the poorest mixing was obtained for the cases where either one of the walls is in the motion or walls are in motion opposing. Furthermore the most rapid mixing was found to occur at low Reynolds' number due to concentration intensity spread out horizontally in the cavity's centre region. This is because of the relatively weak flow induced that lead to greater diffusion. Moreover, the mixing quality was changed by shear thinning effects. It was usually seen that the mixing process for a viscous fluid is faster that viscoelastic fluids. This is because of the fact that mixing of the viscoelastic fluids is slower due to the elastic effect; mixing improves with stronger inertial forces. In this study Weissenberg number Wi of 10^{-3} is used so that the elastic effect was not strong. As a result the findnes for viscous and viscoelastic fluids were in agreement both qualitatively and quantitatively.

When the mixing properties were investigated by tracking the motion of a number of selected fluid particles under discontinuous periodic wall motion it was found that for low Reynolds number the particles followed 'flatter' paths nearer the top plate. Moreover, as Re increases the particle paths become more 'tightly bound' for both viscos and viscoelastic fluids.

Acknowledgement

This is the part of the study which has been carried out at the University of Glamorgan and the author would like to thank Dr. R. W. Williams for this interest and encouragement.

REFERENCES

[1] CROCHET, M.J., DAVIES, A.R. and WALTERS, K.: Numerical Simulation of non-Newtonian Flow. Rheology Series 1. Elsevier 1984.

[2] BIRD, R.B., ARMSTRONG, R.C. and HASSAGER, O.: Dynamics of Polymeric Liquids, Vol. 1. Fluid Dynamics. John Wiley and Sons. New York 1977.

[3] MORGAN, K. et al.: Computer Methods in Fluids. Pentech Press, London: Plymouth 1980.

[4] MORTON, K.Y. and MAYERS, D.F.: Numerical Solution of Partial Differential Equations. Cambridge University Press 1994.

[5] SCRATON, R.E.: Further Numerical Methods in Basic. Edward Arnold 1987.

[6] SMITH, G.D.: Numerical Solution of Partial Differential Equations: Finite Difference Methods. Second Edition. Clarendon Press Oxford 1978.

[7] TOSOKA, N. et al.: Int. J. Solid Structure 31, 1847-1859, 1994.

[8] AREF, H.: J. Fluid Mech. 143 1-21 1984.